33RD CONGRESS
OF THE INTERNATIONAL COUNCIL
OF THE AERONAUTICAL SCIENCES
STOCKHOLM, SWEDEN, 4-9 SEPTEMBER, 2022

ICAS 2022 SWEDEN

# AN EVALUATION METHOD FOR AIRCRAFT ACTUATION SYSTEMS OPERATIONAL COST

Christopher Reichenwallner[1], Felix Larsson[2] & Alessandro Dell'Amico[1,2]

[1]Linköping university, SE-581 83, Linköping, Sweden
[2]Saab AB, SE-581 88, Linköping, Sweden

## Abstract

The transition towards more electrical system architectures can be seen among several aircraft manufacturers. Whether such a transition is suitable for the actuation system is however not apparent and can only be answered with extensive evaluation. A first iteration of a method aimed to structure this evaluation is presented in this paper. Simplistic models for the actuation system and its adjacent systems are introduced and explored in a case study in which a delta-canard aircraft is flown with an hydraulic actuation system. System attributes, such as energy consumption, mass and volume, are evaluated in terms of their respective impact on the fuel burned over a flown mission. The case study indicates that energy efficiency is not one of the main drivers for an electrified actuation system, because of its low impact on the fuel burned during a mission.

**Keywords:** More electric aircraft, Evaluation method, Actuation system, Operational cost

## 1. Introduction

In the wake of more electric aircraft, MEA, electrified actuators, such as the electromechanical actuator, EMA, and the electrohydrostatic actuator, EHA, have emerged as possible replacements for the traditional hydraulic servo actuator, HSA. The transition towards more electrical actuation systems can be observed among several aircraft manufacturers. Airbus adopted a combined hydraulic and electric actuation system architecture on its A380 and employed EHAs on its primary control surfaces, albeit in backup-mode [1]. Boeing chose to install EMAs on a fraction of its spoilers on the B787 [2] and Lockheed Martin uses EHAs on all primary control surfaces on its F-35 [3]. Other projects for proof of concept of the EHA and EMA can be read about in [4] and [5], in which the two actuator technologies were tested and evaluated in the McDonnell Douglas F-18.

The reason behind the transitions to the exact actuation system architectures for the above mentioned aircraft are not obvious. Expectations, such as increased system safety, higher reliability and overall cost benefits, of an electrified actuation system are all but certain for every type of flying platform [6, 7]. The overall platform architecture and the direct use of the actuators may differ considerably between platform types, and the evaluation of the actuation system must account for these differences. Potential aspects to be considered in the evaluation were presented in [8]. The aspects have their origin in Life Cycle Cost and aims to enable and bring forth trade studies among the major life cycle cost contributors. Figure 1 shows the aspect structure presented in [8], here with operational cost in focus. As a continuation of the work presented in [8], this article will cover and bring forth a first iteration of method for the evaluation and analysis of an actuation system's operational cost. The intention for the method is to function as a tool in aircraft conceptual design stages, and by which, incentivize system solutions by their quantified contribution to operational cost.

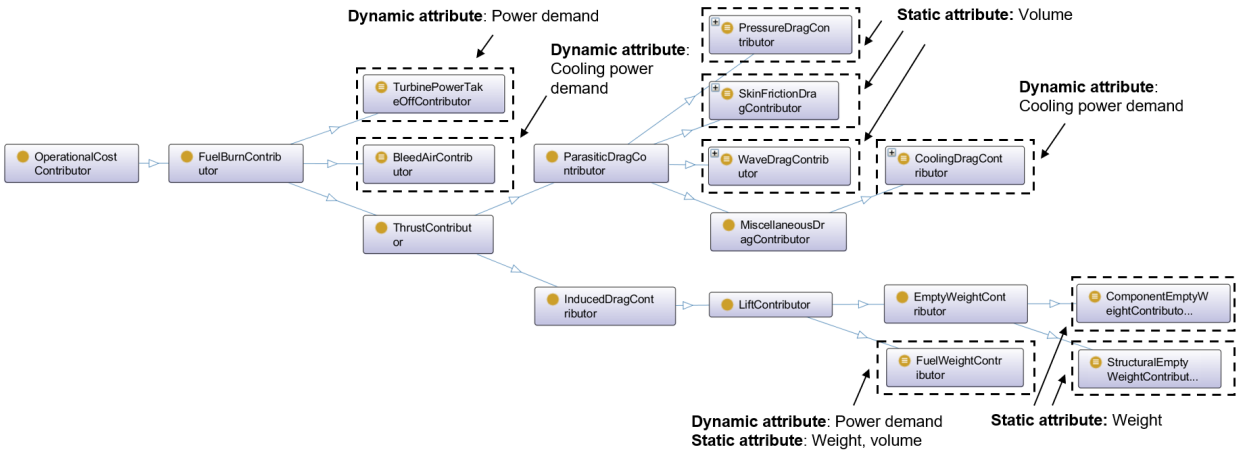


Figure 1 – Evluation aspect hierarchy for operational cost [8].

The outline of the paper is as follows. The method structure with its logical flow of execution, a proposed system decomposition and a general model composition will be presented in Section 2. Section 3 will introduce the models used for the various components included in the above mentioned systems. Section 4 will then showcase the method in a use case in which a delta-canard aircraft is equipped and flown with an hydraulic actuation system. The method and the models are then discussed in Section 5, while Section 6 provides concluding remarks.

## 2. Model overview and method structure

The method in this paper builds on the structure of systems illustrated in Figure 2. Although the actuation system is the system under review, its close coupling to adjacent systems and their influence on the evaluation results cannot be overlooked. The adjacent systems are identified as the distribution, supply and cooling systems. These systems are responsible for the distribution of power, supply of power and management of heat losses respectively. The underlying reason for this decomposition of systems is to gain a more comprehensible view of the influence from each adjacent system. As a reference, the distribution system alone in an Airbus A380 accounts for 75% of the total hydraulic mass, leaving the supply system and actuation system to cover the remaining 25% [2]. This allocation of mass is most certainly different for aircraft of other sizes. It should also be noted that the corresponding mass allocation for an electrical actuation, distribution and supply system for the A380 case has not been found by the author, and the resulting mass allocation may very well look similar.

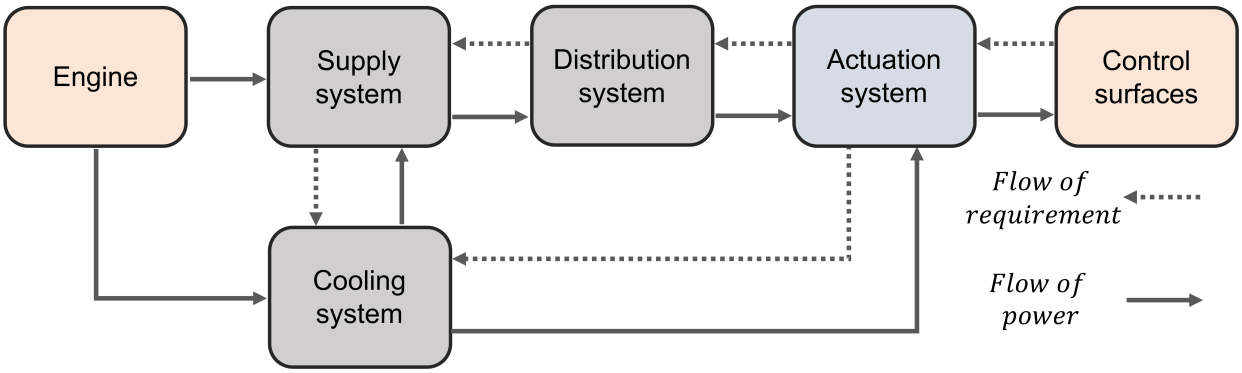


Figure 2 – System level decomposition. The actuation system is under review. The distribution, supply and cooling systems must be included in the evaluation as well. The engine and control surface design are assumed fixed.

The constituent components in each system are modeled using a functional approach. It is proposed to describe a component in terms of its primary and secondary functional requirements, system and component design parameters and static and dynamic attributes, as suggested in Figure 3.

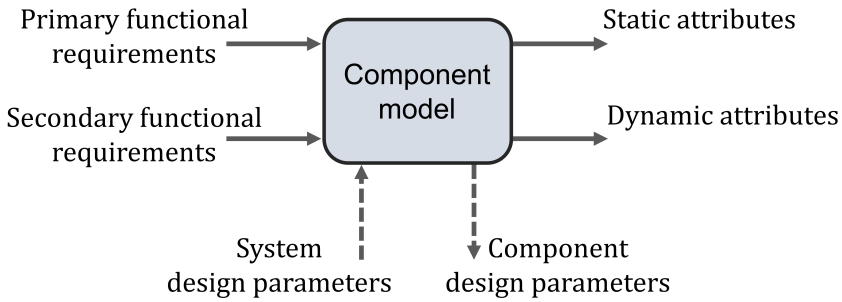


Figure 3 – Component model structure

The definition of the concepts are as follows:

- **Primary functional requirements -** Requirements related to the primary function of a component. I.e, the actuating function of an actuator.
- **Secondary functional requirements -** Requirements related to various secondary functions of a component. I.e, the function of locking a load in place for an actuator or the function of isolating a leakage in a hydraulic distribution system.
- **System design parameters -** System defined quantities that will impact the design of a component. I.e, system pressure levels or available coolant mass flow.
- **Component design parameters -** Quantities that describe the design of a component. I.e, the effective area of a cylinder or the lead of a ball screw.
- **Static attributes -** Time-invariant attributes of a component. I.e, component mass and dimensions. Relevant for aircraft integration.
- **Dynamic attributes -** Time-variant attributes of a component. I.e, supply power demand and cooling power demand. Relevant for adjacent systems.

There exist a mapping between the different concepts presented above, such that for a given set of component design parameters there exist a set of static and dynamic attributes. This mapping will naturally become more accurate the further a component (or system) is decomposed, simply because of a decreased number of possible component architectures. Therefore, this mapping can naturally be constructed with various levels of fidelity, with the lowest level being a direct mapping between the performance requirements of a function and the attributes of the component.

This paper will mainly focus on the primary functions in this first iteration of the method. Furthermore, the mapping used between functions and attributes will also be composed with varying levels of fidelity and without any particular motivation for the chosen level. The underlying reason is mainly the lack of easily obtained data for aircraft components.

## 2.1 Logical flow of execution

The aircraft systems, decomposed as presented in Figure 2, are integrated into a simulation environment on the format visualized in Figure 4. System control references are computed by a control system and sent to the aircraft system models. The states of the aircraft systems are calculated and advanced to an aircraft model which solves the aircraft equations of motion and return the aircraft

states. The aircraft model is also provided with the system static attributes in order to capture how these change the configuration of the aircraft when integrated into it. Aerodynamic loads from the aircraft model are fed back to the system models and the system models eventually outputs the measure of performance, in this case the cumulative fuel consumption, as indicated in the hierarchy in Figure 1.

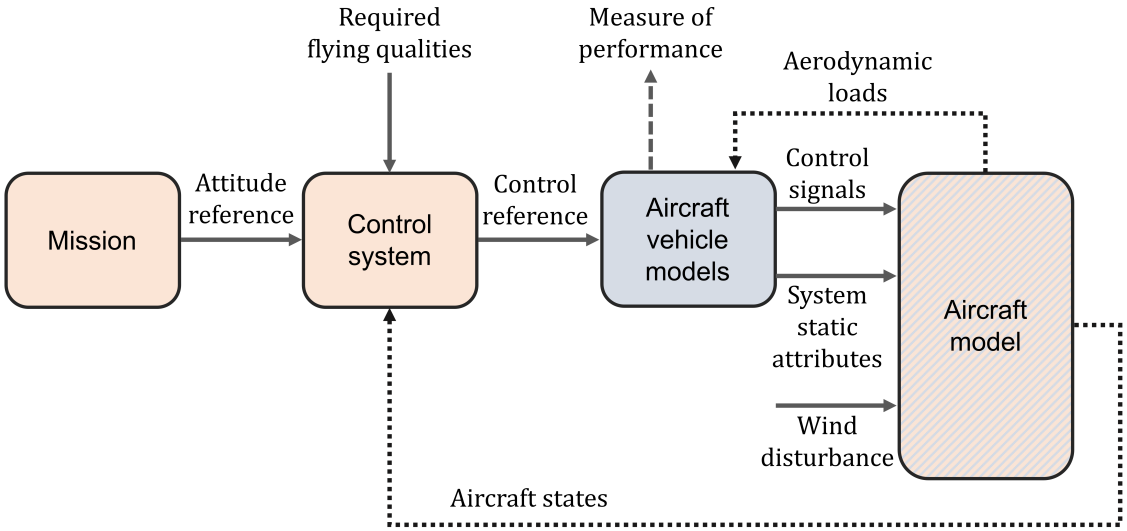


Figure 4 – Simulation environment including a control system, the aircraft vehicle systems and an aircraft model.

The logical flow of execution starts with building the system architectures, i,e., every actuator component, distribution component, supply component and cooling component in accordance with design rules and safety regulations. One mission is simulated without any systems in order to determine the performance requirements on the actuation system. The actuation system is then evaluated in terms of design parameters before its attributes are evaluated in a second simulation. This simulation will thereby generate the performance requirements posed on the remaining systems. A third simulation will evaluate the design parameters and attributes of these remaining systems. A possible iteration of the last 3 steps is now possible, and needed, if the performance requirements for actuation of the aircraft have changed because of a changed aircraft configuration.

## 3. System models

This section presents the underlying theory for the models used in the evaluation. Models for two categories of systems, one hydraulic and one electric, will be presented. The hydraulic category will cover a traditional hydraulic servo actuation system with its adjacent systems and the electric category will cover an electromechanical actuation system with its adjacent systems.

### 3.1 Actuation system models - Hydraulic servo actuator

An HSA, in its most basic form, is composed of one hydraulic cylinder and one control valve. The following expressions are used to estimate its component design parameters:

$$d_p = \left( \frac{4 \cdot F_{stall}}{\pi \cdot n_A} \frac{1}{p_{sup} - p_{ret}} \frac{1}{1 - AR} \right)^{1/2} \tag{1}$$

$$A_v = \omega \cdot x_{v,max} = \frac{A_p \cdot V_{max}}{C_q \cdot \sqrt{\frac{2}{\rho_f} \cdot \Delta p_{nom}}} \tag{2}$$

Where for Equation 1, $F_{stall}$ denotes the actuator stall force. $p_{sup}$, $p_{ret}$ and $n_A$ are the supply pressure, return pressure and a parameter describing how the load is divided between all actuators acting on the load. Lastly, $AR$ denotes an assumed ratio between piston area and rod area. For Equation 2,

$V_{max}$ denotes the actuator maximum velocity, $\omega$ and $x_{v,max}$ are the valve area gradient and maximum spool position respectively, $A_p$ the effective cylinder piston area obtained from $d_p$ and $AR$, $C_q$ the valve flow coefficient, $\Delta p_{nom}$ the pressure drop at which maximum velocity is to be achieved and $\rho_f$ the oil density.

The HSA static attributes are identified as its mass, length, width and height. The mass is estimated using the following growth model based on two samples of hydraulic servo actuators from the Saab 2000 aircraft.

$$m_{HSA} = F_{stall} \cdot 2.51 \cdot 10^{-5} + 9.18 \tag{3}$$

The dimensions are assumed to be represented by the hydraulic cylinder only. This is a rough estimation since the influence of where the valve is installed and also all possible secondary functions of the actuator are neglected. The following expressions are used for the estimation:

$$L_{HSA} = B_{HSA} + S \tag{4}$$

Where $B_{HSA}$ is the base length and $S$ the stroke. The base length is estimated as a function of the stroke. The following growth model, based on values of stroke and length on hydraulic cylinders of the brand MTS is used for the base length. The type of cylinder will also matter.

$$B_{HSA} = \begin{cases} S \cdot 2.03 + 0.4, & \text{Simplex cylinder} \\ S \cdot 3.03 + 0.4, & \text{Tandem cylinder} \end{cases} \tag{5}$$

Since the installed valve location is neglected, the height and width of the actuator are assumed equal and described as a function of the piston diameter:

$$H_{HSA} = 1.4 \cdot d_p \tag{6}$$

$$W_{HSA} = H_{SHA} \tag{7}$$

The dynamic attributes are estimated using a simulation model on the form presented in Figure 5. The HSA power consumption is mainly dominated by throttling losses in the control valve and leakage. A static model is therefore considered sufficient in order to capture the dynamic attributes of this type of actuator. The following expressions are used to describe the system, $G_x$.

$$p_l = \frac{F_l}{A_p \cdot n_A} \tag{8}$$

$$q_{cyl} = A_p \cdot \dot{x} \tag{9}$$

$$q_{cyl} = C_q \cdot x_v \cdot \omega \cdot \sqrt{\frac{1}{\rho_f} \cdot (p_{sup} - p_l)} \tag{10}$$

Transforming the expressions above to the Laplace domain and solving for $x$ yields the following transfer function:

$$x = \left( x_v \cdot \frac{K_q}{A_p} - F_l \cdot \frac{K_c}{A_p^2} \right) \frac{1}{s} \tag{11}$$

Where $x_v$ is the control signal and represents the valve position, $K_q = \frac{\partial q_{cyl}}{\partial x_v}$ and $K_c = \frac{\partial q_{cyl}}{\partial p_l}$ the valve flow gain and flow pressure coefficient respectively, $F_l$ the load force and $s$ the Laplace operator. The supply flow per actuator is lastly described using:

$$q_{sup} = q_{cyl} + q_l \tag{12}$$

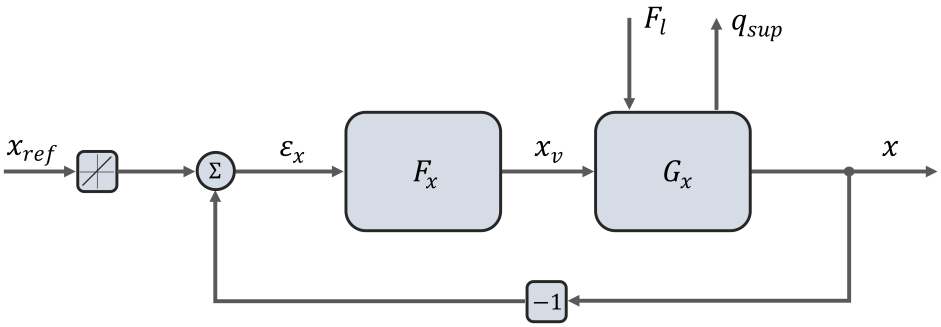


Figure 5 – HSA simulation model format

Where $q_l$ denotes the valve leakage, which can be included in the model if it is desirable to capture the parasitic influence of leakage on energy consumption as well.
The proposed model includes a position control loop with controller, $F_x$. The controller is designed for the closed loop performance to be approximated as a first order system with time constant $T_{x,c}$, which gives:

$$G_{x,c} = \frac{F_x \cdot G_x}{1 + F_x \cdot G_x} = \frac{1}{T_{x,c} \cdot s + 1} \tag{13}$$

Solving for $F_x$ yields:

$$F_x = \frac{A_p}{K_q \cdot T_{x,c}} \tag{14}$$

Hence, a pure proportional controller.

## 3.2 Actuation system models - Electromechanical actuator model

The electromechanical actuator is composed of, in its most basic form, one ball screw (or similar gear), one electric motor and one motor controller. The ball screw lead is estimated using the following expression:

$$K_l = \frac{V_{max}}{\omega_{m,max}} \cdot 2\pi \tag{15}$$

Where $\omega_{max}$ is an assumed maximum motor rotational speed. The back EMF constant, and thus the torque constant, of the motor is estimated using:

$$K_e = K_t = \frac{U_{sup}}{\omega_{m,max}} \tag{16}$$

Where $U_{sup}$ denotes the supply voltage. The motor winding resistance, $R_m$ is estimated using the expression below. The expression is derived from the motor constant, $K_m$, which is an efficiency measure of how well the electric motor is able to convert electric power into torque. Typical values of the constant can be derived from electric motor datasheets.

$$K_m = \frac{T_m}{\sqrt{P_{m,loss}}} \tag{17}$$

With $P_{m,loss} = R_m \cdot i_m^2$ and $T_m = K_t \cdot i_m$ the following equation is obtained:

$$K_m = \frac{K_t \cdot i_m}{\sqrt{R_m \cdot i_m^2}} \tag{18}$$

Solving for $R_m$ yields

$$R_m = (\frac{K_t}{K_m})^2 \tag{19}$$

Where $T_m$ denotes the motor torque, $P_{m,loss}$ the resistive losses in the motor and $i_m$ the motor current. The rotor inertia is estimated using the growth model below. The growth model is based on rotor inertia values from permanent magnet synchronous machines of the brand Baumüller.

$$J_m = T_{stall}^{1.6} \cdot 6.47 \cdot 10^{-2} \tag{20}$$

Where $T_{stall}$ is the motor maximum torque and is found from the relation between stall force and ball screw lead:

$$T_{stall} = F_{stall} \cdot \frac{K_l}{2\pi} \tag{21}$$

The EMA static attributes are identified as its mass, length, width and height. The growth model below is used to estimate the mass of the EMA. The growth model is a linear regression model on force to mass based on the EMAs found in [5, 9, 10, 11].

$$m_{EMA} = F_{stall} \cdot 3.72 \cdot 10^{-4} + 5.11 \tag{22}$$

The EMA dimensions are estimated using the expressions below. Similar to the HSA, the dimensions are assumed to be represented by the electric motor and ball screw only. The motor controller will have a significant contribution to the total volume of the actuator setup, but its location for installation can vary. The following expressions, based on the EMA data found in [5, 9, 10, 11], are used to estimate the dimensions:

$$L_{EMA} = B_{EMA} + S \tag{23}$$

$$B_{EMA} = S \cdot 3.11 + 0.19 \tag{24}$$

$$H_{EMA} = F_{stall} \cdot 1.49 \cdot 10^{-6} + 0.09 \tag{25}$$

$$W_{EMA} = H_{EMA} \tag{26}$$

The dynamic attributes of the EMA are estimated using a simulation model on the form presented in Figure 6. The EMA power loss is assumed to be dominated by resistive losses in the electric motor and power controller. The rotor inertia will however also play a significant roll in the total energy consumption of the actuator. Frequent accelerations of the actuator will result in frequent energy losses due to the inability of recuperating the energy stored in the rotating part of the actuator. The behavior of the EMA assumed to be dominated by this inertia while the dynamics of the electromagnetic torque are considered to be sufficiently fast, with respect to the mechanical time constant, to be neglected. The model is inspired by the proposed EMA model found in [12]. The rotor torque equilibrium is used to describe the system $G_\omega$:

$$T_m = T_l + B_m \cdot \omega_m + J_m \cdot \dot{\omega}_m \tag{27}$$

Transforming the expression to the Laplace domain and solving for $\omega$ yields:

$$\omega_m = \frac{T_m - T_l}{B_m + J_m \cdot s} \tag{28}$$

Where $T_l$ the load torque and $B_m$ the rotor damping coefficient. The load torque is solved from the relation between torque, force and ball screw lead as:

$$T_l = F_l \cdot \frac{K_l}{2\pi} \tag{29}$$

Further, the system $G_x$ is described using:

$$G_x = \frac{1}{s} \cdot \frac{K_l}{2\pi} \tag{30}$$

Hence a pure integrator and conversion to linear motion from rotational. The supply current per actuator can lastly be estimated as:

$$i_{sup} = \frac{i_m \cdot (U_m + U_i)}{n_A \cdot U_{sup}} \tag{31}$$

Where $U_m$ is the voltage drop over the motor windings and $U_i$ is the voltage over the motor controller. The voltage drop over the motor windings is estimated using the equation of an equivalent DC armature circuit as:

$$U_m = R_m \cdot i_m + K_e \cdot \omega_m \tag{32}$$

The motor current is estimated using:

$$i_m = \frac{T_m}{K_t} \tag{33}$$

The voltage drop over the motor controller is lastly found through:

$$U_i = R_i \cdot i_m \tag{34}$$

Where $R_i$ is the motor controller resistance.

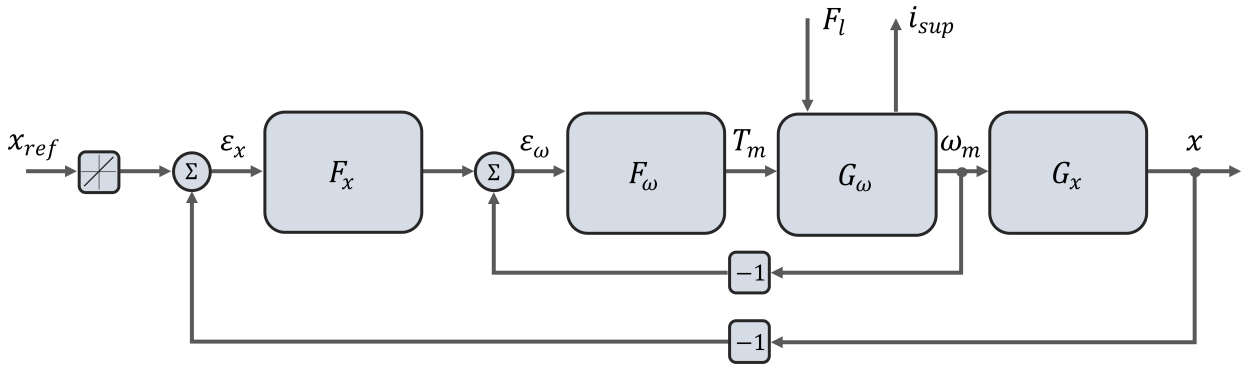


Figure 6 – EMA simulation model format

The EMA model includes one inner speed loop and one outer position loop. Similarly to the HSA model, the position loop controller is designed for the closed position loop performance to be approximated as a first order system with time constant $T_{x,c}$. The closed speed loop performance is also approximated as a first order system, but with time constant $T_{\omega,c}$. There is generally no performance requirement on a system level determining the value of $T_{\omega,c}$. As a best practice it is however considered to dimension $T_{\omega,c}$ to meet the following condition:

$$T_{x,c} \cdot 10 \leq T_{\omega,c} \leq T_s \cdot 0.1$$

Where $T_s$ is the simulation sample time. The closed speed loop is given by:

$$G_{\omega,c} = \frac{F_\omega \cdot G_\omega}{1 + F_\omega \cdot G_\omega} = \frac{1}{T_{\omega,c} \cdot s + 1} \tag{35}$$

Solving for $F_\omega$ yields:

$$F_\omega = \frac{J_m}{T_{\omega,c}} \left(1 + \frac{1}{T_\omega}\right) \tag{36}$$

Hence, a proportional-integral controller in which $T_\omega$ is the time constant of the system $G_\omega$. The time constant is given by:

$$T_\omega = \frac{J_m}{B_m} \tag{37}$$

The closed position loop is lastly given by:

$$G_{x,c} = \frac{F_x \cdot G_{\omega,c} \cdot G_x}{1 + F_x \cdot G_{\omega,c} \cdot G_x} = \frac{1}{T_{x,c} \cdot s + 1} \tag{38}$$

Solving for $F_x$ yields:

$$F_x = \frac{T_{\omega,c}}{T_{x,c}} \left( \frac{1}{T_{x,c}} + s \right) \tag{39}$$

Hence, a proportional-derivative controller.

### 3.3 Distribution system models - Hydraulic transmission line model

The distribution system components will only be explained in terms of their design parameters and static attributes. The dynamic attributes are considered to have low to no impact on the total power consumption of the system. This applies to both categories of distribution components. Furthermore, the distribution components are assumed to be represented by the transmission lines only. Other components for secondary functions, such as fuses for isolation of faults and accumulators for equalization of pulsations, are yet to be implemented in the models.

The design parameters for the hydraulic line are identified as its inner and outer pipe diameter. The inner diameter of the pipe can be estimated as a function of the maximum allowed power loss over a distance. The following equations are used:

$$P_{loss} = \varepsilon \cdot P_{trans} = R_{hyd} \cdot q_{sup}^2 \tag{40}$$

Where $\varepsilon$ represent the relative power loss, $P_{trans}$ the transmitted power, $R_{hyd}$ the hydraulic resistance and $q_{sup}$ the supplied hydraulic flow to the consumer. Assuming laminar flow, the resistance can be expressed as:

$$R_{hyd} = \frac{128 \cdot \eta_f \cdot l}{\pi \cdot d_i^4} \tag{41}$$

Where $\eta_f$ is the dynamic viscosity of the fluid, $l$ the distance between supplier and consumer and $d_i$ the inner diameter of the pipe. Solving Equation 40 and 41 for $d_i$ yields:

$$d_i = \left( \frac{q_{sup}}{\varepsilon \cdot p_{sup}} \frac{128 \cdot \eta_f \cdot l}{\pi} \right)^{1/4} \tag{42}$$

The thickness of the pipe can then be found through Hoops stress law. Solved for the outer diameter, $d_o$ gives the following expression:

$$d_o = d_i \left( 1 + \frac{P_{max}}{\sigma} \right) \tag{43}$$

Where $\sigma$ is the yield strength of the pipe material and $P_{max}$ is the maximum peak pressure in the system. The mass of the hydraulic transmission line is a function of the pipe mass and the mass of the contained hydraulic fluid. Assuming the same dimensions on the return line as on the supply line, the following expression is obtained:

$$m_{h,line} = (m_p + m_f) \cdot 2 = l \frac{\pi}{2} \left( (d_o^2 - d_i^2) \cdot \rho_p + d_i^2 \cdot \rho_f \right) \tag{44}$$

Where $\rho_p$ and $\rho_f$ denotes the density of the pipe material and the density of the fluid respectively. The total volume of the transmission line is simply a function of its outer dimensions.

## 3.4 Distribution system models - Electric transmission line model

The design parameters for the electric transmission line are estimated similarly to those of the hydraulic line. The following equation for power loss is valid for the electric transmission line:

$$P_{loss} = \varepsilon \cdot P_{trans} = R_{el} \cdot i_{sup}^2 \tag{45}$$

Where $R_{el}$ is the electric resistance and $i_{sup}$ the current supply to the consumer. The electric resistance is estimated from:

$$R_{el} = \frac{4}{\pi \cdot d_i^2} \cdot \rho_e \cdot l \tag{46}$$

Where $\rho_e$ in this context denotes the resistivity of the conductive material. Solving Equation 45 and Equation 46 for $d_i$ yields:

$$d_i = 2 \cdot \left( \frac{\rho_e \cdot l \cdot i_{sup}}{\pi \cdot \varepsilon \cdot U_{sup}} \right)^{1/2} \tag{47}$$

The outer diameter becomes a function of the inner diameter and insulation thickness of the electric line:

$$d_o = d_i + 2 \cdot t \tag{48}$$

Where $t$ is the insulation thickness. The mass of the electric line is calculated similarly to the hydraulic line but as a function of the conductor material properties and insulation material properties instead. With the same dimensions on the return line, the following expression is obtained:

$$m_{e,line} = (m_c + m_i) \cdot 2 = l \frac{\pi}{2} \left( (d_o^2 - d_i^2) \cdot \rho_i + d_i^2 \cdot \rho_c \right) \tag{49}$$

Where $\rho_i$ and $\rho_c$ denotes the density of the insulation material and the density of the conductive material respectively. The total volume of the transmission line is simply a function of its outer dimensions.

## 3.5 Supply system models - Hydraulic supply unit

The supply system models are not represented using the concept of design parameters. The static attributes are instead directly correlated with the performance requirements using growth models while the dynamic attributes are estimated using a static value of an efficiency. These models can therefore be considered of very low fidelity level.

A supply unit for the hydraulic supply is regarded as an hydraulic pump and an oil reservoir. The pump mass and volume are estimated using the following growth models:

$$m_{pump} = P_{pump} \cdot 11.46 \cdot 10^{-2} + 1 \tag{50}$$

$$V_{pump} = P_{pump} \cdot 4.21 \cdot 10^{-5} + 9.70 \cdot 10^{-4} \tag{51}$$

Where $P_{pump}$ is the maximum output power from the pump. The models are based on pump data from Bosch Rexroth and adapted to fit one pump sample from the Saab 2000 aircraft. The oil reservoir mass och volume are estimated using:

$$m_{res} = V_{hyd} \cdot 0.3 \cdot 2 \cdot 10^{-3} \tag{52}$$

$$V_{res} = V_{hyd} \cdot 0.3 \tag{53}$$

Where $V_{hyd}$ corresponds to the total enclosed oil volume in the complete hydraulic system. The mass growth model for the reservoir is based on the work in [13], in which the reservoir volume is argued

to equal 30% of the total enclosed system volume. The volume of the reservoir simply assumes to equal the volume it encloses. Lastly, the dynamic attributes are estimated using:

$$P_{in,sup} = \frac{P_{out,sup}}{\eta_{sup}} \tag{54}$$

## 3.6 Supply system models - Electric supply unit

The static attributes of the electric supply unit are, similarly to the hydraulic supply unit, directly correlated to its performance requirements. The following growth models are based on electric machine data from Baumüller.

$$m_{gen} = P_{gen} \cdot 1.66 \cdot 10^{-3} - 4 \tag{55}$$

$$V_{gen} = P_{gen} \cdot 0.55 \cdot 10^{-6} - 0.70 \cdot 10^{-3} \tag{56}$$

Where $P_{gen}$ is the maximum power output from the generator. The dynamic attributes are estimated using Equation 54

## 3.7 Cooling system models - Fuel heat exchanger

The fuel heat exchanger, assumed to be used by the hydraulic actuation system, is described by its static attributes only. The component is passive by nature and relies on an already existing flow of either hydraulic oil or fuel. The following expressions for the mass and volume are used:

$$m_{FHE} = \overline{P}_{cool} \cdot \frac{10^{-3}}{0.5} \tag{57}$$

$$V_{FHE} = \overline{P}_{cool} \cdot \frac{10^{-3}}{0.300} \tag{58}$$

Where $P_{cool}$ is the mean required cooling power and is regarded as a performance requirement. This performance requirement is heavily affected by how the equipment, in need of cooling, is used. The values of the specific mass and volume comes from industry data.

## 3.8 Cooling system models - Air cycle machine

The air cycle machine, assumed to be used by the electric actuation system, is described by its static and dynamic attributes. Since the electric actuation system cannot transport heat losses away from the its source, it relies on being actively supplied with cooling power. The static attributes are estimated using:

$$m_{ACM} = \overline{P}_{cool} \cdot \frac{10^{-3}}{0.2} \tag{59}$$

$$V_{ACM} = \overline{P}_{cool} \cdot \frac{10^{-3}}{0.100} \tag{60}$$

The dynamic attribute is identified as the coolant mass flow, $\dot{m}$ and is estimated using the relation between requested cooling power, $\dot{Q}$, specific heat capacity of air, $C_p$ and an assumed temperature difference over the object being cooled, $\Delta T$.

$$\dot{m} = \frac{\dot{Q}}{C_p \cdot \Delta T} \tag{61}$$

## 3.9 Aircraft configuration models

In accordance with the hierarchy presented in Figure 1, integrating equipment into the aircraft will change the aircraft configuration. Mass from installed equipment can commence snowballing effects on structural mass while volume from equipment may require changes in aircraft shape. This will in turn overshadow the operational costs of the aircraft. Aircraft shape configurations will be covered in this article by the inclusion of a model for estimation of fairing drag. Aircraft are often proven to be too small for the equipment installed in it. Either because of inadequate anticipation of equipment size during conceptual design or simply as a consequence of aircraft type. Protruding parts from the aircraft body can therefore be covered with fairings (also known as blister), but at the expense of aerodynamic drag.

Examples of fairings associated with the actuation system can easily be observed on aircraft such as the Lockheed Martin's F22 Raptor, the Suchoj's SU-57 or the McDonnell Douglas's F18 Super Hornet. Each elevon control surface employs a fairing to cover the actuator as it is too large to fit in the wing profile. In literature, this aerodynamic penalty is rarely accounted for when evaluating aircraft actuation systems.

The correlation between fairing size and its contribution to the total basic drag of an aircraft is poorly studied in literature. A modest method for estimating this contribution in early conceptual design is given by [14]. This method is adopted from [15] which in turn summarized the, for the public, brief available experimental data. Another, slightly more elaborated methodology is provided by ESDU and can be found in [16]. This method has been employed in this work and will briefly be explained.

ESDU suggest the following expressions for fairing drag estimations.

$$\frac{C_D}{(C_D)_{\delta=0}} = \begin{cases} \frac{1}{1+m} \cdot \left(\frac{h}{\delta}\right)^m, & \frac{\delta}{h} \geq 1 \\ \left(1-\frac{\delta}{h}\right) + \frac{1}{1+m} \cdot \frac{\delta}{h}, & \frac{\delta}{h} < 1 \end{cases} \tag{62}$$

Where $C_D$ denotes the resulting drag coefficient for the fairing, $(C_D)_{\delta=0}$ the drag coefficient for the fairing in absence of the aircraft boundary layer, $m$ a power index for the shape of the fairing, $h$ the height of the fairing and $\delta$ the height of the boundary layer. See Figure 7 for a visual reference. The equations are based on measured data from wind tunnel testing where the upper equation is valid for fairings submerged in the boundary layer of the aircraft surface and the lower equation is valid for fairings higher than the boundary layer. It can be observed in the equations that as the fairing height increases and exceed that of the aircraft surface boundary layer, the fairing drag will increasingly assume the value of its corresponding drag in free stream.

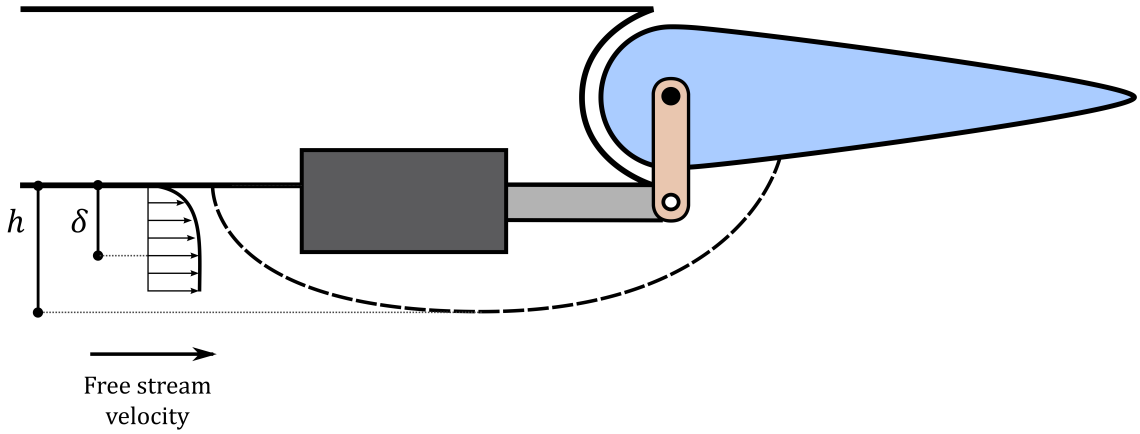


Figure 7 – Illustration of a wing-mounted actuator inside of a fairing.

The value of the power index, $m$, can be estimated using the following equations.

$$m = \begin{cases} 1.1765 \cdot \left(\frac{h}{\delta}\right), & M \leq 0.8 \text{ and } \frac{h}{\delta} \leq 0.85 \\ -0.0839 \cdot \left(\frac{h}{\delta}\right) + 0.3094, & M = 1.4 \text{ and } \frac{h}{\delta} \leq 1 \\ -0.0894 \cdot \left(\frac{h}{\delta}\right) + 0.3643, & M = 2.2 \text{ and } \frac{h}{\delta} \leq 1 \\ -0.0787 \cdot \left(\frac{h}{\delta}\right) + 0.4750, & M = 2.8 \text{ and } \frac{h}{\delta} \leq 1 \end{cases} \tag{63}$$

Where $M$ is the mach number. For $\left(\frac{h}{\delta}\right)$ greater than the above defined upper boundaries, i.e, 0.85 and 1, the value of the quota will simply assume the value of the upper boundary. It can also be observed that the estimation of $m$ is undefined in the transonic regime. A simple linear estimation between $M = 0.8$ and $1.4$ is therefor used.

The fairing drag in absence of boundary layer, $(C_D)_{\delta=0}$, is estimated using the methods provided in the following ESDU documents [17, 18]. The documents offer drag estimations for several different geometrical shapes. [17] is used to estimate the geometrical coefficients for a chosen shape based on its dimensions, in this case the shape of the fairing, and [18] is then used to estimated the corresponding profile drag based on the body geometry and as a function of mach number.

## 4. Results

This section will cover some preliminary results using the above explained models and method. The results will be shown for one hydraulic actuation system employing tandem actuators on all control surfaces. The actuators are supplied by two separated hydraulic supply and distribution systems. Cooling is ensured by fuel heat exchangers, one for each hydraulic system. To more easily comprehend the results from the study, this section will be structured to firstly present the aircraft and mission used in the study. This is followed by a presentation of component data exemplified using one component from each system. The resulting total attributes for each system will then be summarized before their impact on the measure of performance, i.e. fuel burn, is presented.

### 4.1 Aircraft and mission

The evaluation is done using an aircraft simulation model named The Aero-Data Model in a Research Environment (ADMIRE). This model is developed by the Swedish Defense Research Agency with the aim to serve the research environment with an aircraft model that could be freely distributed. The ADMIRE model is implemented in Matlab/Simulink and consist of an nonlinear aircraft simulation model accompanied with a flight control system for stability and sufficient aircraft flying qualities. The aircraft is a small single-seat fighter with delta canard configuration. The aerodynamic data is based on the Generic Aerodata Model (GAM), developed by Saab AB. More information about the aircraft is found in [19].

The mission used for the evaluation example is found in Figure 8. It contains segments of both subsonic and supersonic speeds on intermediate to high altitudes. This mission is however not the reference mission for the actuator performance requirements. The performance requirements are instead found from single maneuvers with high load factor in demanding areas of the flight envelope.

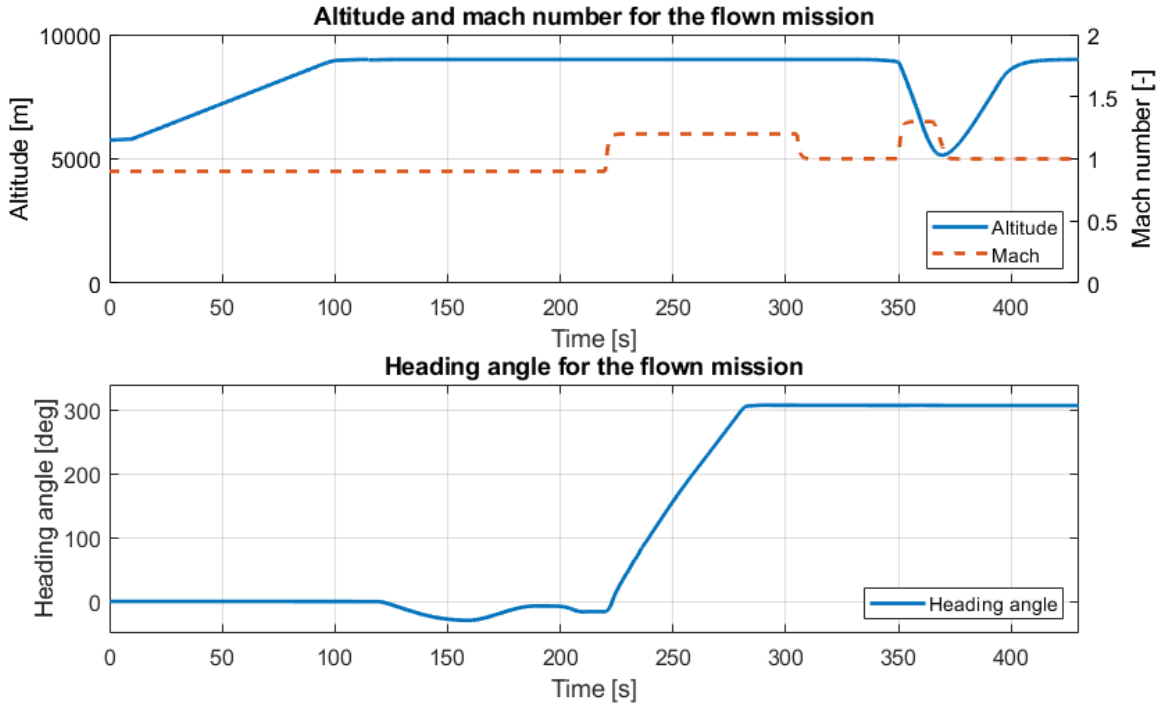


Figure 8 – The flown mission in the case study.

## 4.2 Component and system static attributes

Table 1 summarizes the parameters for the different model concepts (performance requirements, design parameters, static attributes) for one component from each system. The parameters are obtained from following the steps presented in Section 2 and using the models presented in Section 3. To display the parameters for every component in every system would be infeasible in this paper, similar parameters does however exist for the remaining components in each system.

The set of actuator parameters given in Table 1a is an example for the right outer elevon actuator. The stall force is a result of the aerodynamic loading found in the reference mission, as stated earlier. Requirements on rate and response comes from the control system as a consequence of the desired flying qualities. As previously mentioned, the actuator has a tandem configuration, which means that the load is equally shared between two pistons in the same housing. The outer diameter will become slightly smaller as a result of this configuration, but the base length will increase. This actuator is supplied through the transmission line presented in Table 1b. The transmission line maximum pressure is set to four times the supply pressure and titanium is assumed to be used as pipe material. The mass and volume is valid for both the supply and return line. Lastly, the parameters for the supply and cooling units are given in Table 1c and 1d. All static attributes are rounded to their nearest integer.

Summarizing all static attributes for every component in every system yields the results shown in Table 2. The actuation system cover more than half of the total mass and volume of these systems. The remaining systems cover similar fractions of volume but diverge slightly in terms of mass, with the cooling system claiming the smallest fraction of mass.

Table 1 – Component static attributes

(a) HSA parameters - Right outer elevon

| Concept | Variable | Value | |
|---|---|---|---|
| Performance requirements | $F_{stall}$ | 250 | $kN$ |
| | $V_{max}$ | 87.26 | $mm/s$ |
| | $T_{c,x}$ | 0.05 | $s$ |
| Design parameters | $n_a$ | 2 | $-$ |
| | $p_{sup}$ | 280 | $bar$ |
| | $p_{ret}$ | 6.50 | $bar$ |
| | $S$ | 87.30 | $mm$ |
| | $AR$ | 0.50 | $-$ |
| | $\rho_f$ | 850 | $kg/m^3$ |
| | $x_{v,max}$ | 1 | $mm$ |
| | $\omega$ | 3.18 | $mm$ |
| | $d_p$ | 10.79 | $cm$ |
| | $q_l$ | 1 | $l/min$ |
| Static Attributes | $m_{HSA}$ | 15 | $kg$ |
| | $V_{HSA}$ | 14 | $l$ |
| | $B_{HSA}$ | 53 | $cm$ |
| | $L_{HSA}$ | 62 | $cm$ |
| | $W_{HSA}$ | 15 | $cm$ |

(b) Hydraulic transmission line parameters - Right outer elevon

| Concept | Variable | Value | |
|---|---|---|---|
| Performance requirements | $P_{loss}$ | 1 | $\%$ |
| | $q_{sup}$ | 24 | $l/min$ |
| | $p_{sup}$ | 280 | $bar$ |
| Design parameters | $\eta$ | 0.13 | $Ns/m$ |
| | $l$ | 4 | $m$ |
| | $\rho_p$ | 4500 | $kg/m^3$ |
| | $p_{max}$ | 1120 | $bar$ |
| | $\sigma$ | 830 | $MPa$ |
| | $d_i$ | 13.19 | $mm$ |
| | $d_o$ | 14.97 | $mm$ |
| Static attributes | $m_{h,line}$ | 2 | $m$ |
| | $V_{h,line}$ | 1 | $l$ |

(c) Supply unit parameters

| Concept | Variable | Value | |
|---|---|---|---|
| Performance requirements | $q_{sup}$ | 110 | $l/min$ |
| | $p_{sup}$ | 280 | $bar$ |
| Design parameters | $\eta_{sup}$ | 0.85 | $-$ |
| | $V_{hyd}$ | 5.10 | $l$ |
| Static attributes | $m_{pump}$ | 7 | $kg$ |
| | $m_{res}$ | 3 | $kg$ |
| | $V_{pump}$ | 3 | $l$ |
| | $V_{res}$ | 5 | $l$ |

(d) Cooling unit parameters

| Concept | Variable | Value | |
|---|---|---|---|
| Performance requirements | $\overline{P}_{cool}$ | 2.4 | $kW$ |
| Static attributes | $m_{FHE}$ | 4 | $kg$ |
| | $V_{FHE}$ | 8 | $l$ |

Table 2 – Total system static attributes

| | Actuation sys. | Distribution sys. | Supply sys. | Cooling sys. | Total |
|---|---|---|---|---|---|
| **Mass** | 96 $kg$ | 25 $kg$ | 20 $kg$ | 9 $kg$ | 150 $kg$ |
| **Volume** | 77 $l$ | 15 $l$ | 17 $l$ | 16 $l$ | 125 $l$ |
| **Rel. mass** | 64.00 % | 16.67 % | 13.33 % | 6.00 % | |
| **Rel. volume** | 61.60 % | 12.00 % | 13.60 % | 12.80 % | |

## 4.3 Component and system dynamic attributes

Figure 9 shows the right outer elevon velocity and applied force over the flown mission. A constant movement of the actuator can be noticed and is the result of the flight control system's suppression of wind disturbances acting on the aircraft. It can be observed that the output power remains on low levels. The mean output power amounts to approximately $3.8\ W$ and the peak power to approximately $2.8\ kW$. All other actuators in the system show similar numbers. The more interesting quantity is however the required input power needed to meet this low output power. This is illustrated in Figure 10. The input power is valid for the entire system chain and is thus a representation of the mechanical power extracted from the engine shaft. The mean input power amounts to approximately $4.7\ kW$ (comparable with the mean cooling power in Table 1d) and peaks at approximately $103.5\ kW$. A small offset can be noticed in the figure. This offset is a result of the valve leakage, which, for $1\ l/min$ per actuator, amounts to approximately $3.2\ kW$ of power. In other words, $68\ \%$ of the mean input power is consumed only by leakage and the cooling unit is therefore sized almost individually for the sake of leakage.

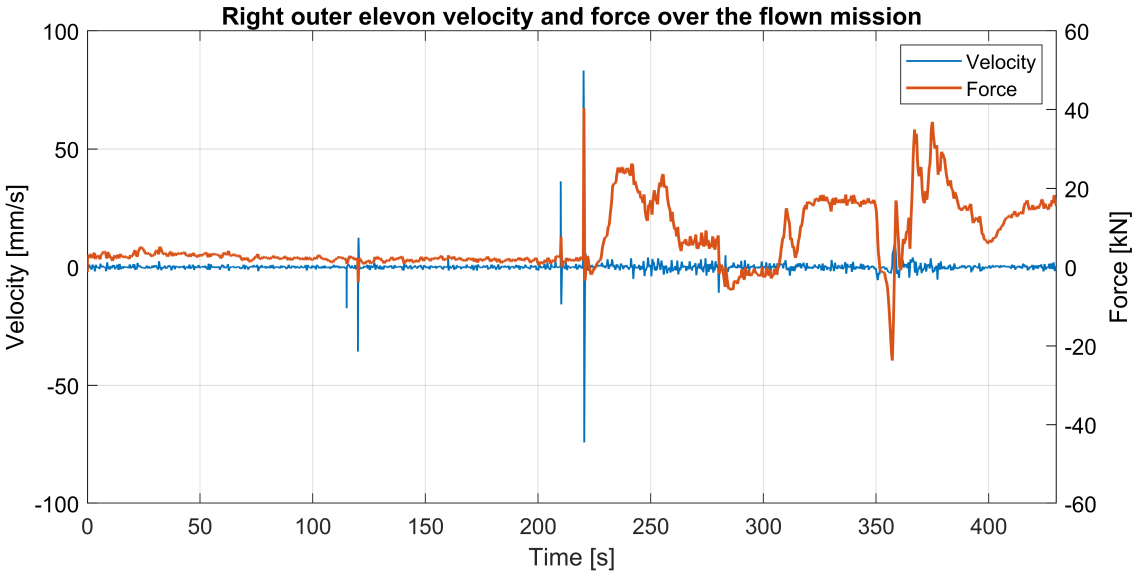


Figure 9 – Velocity and force for the right outer elevon actuator.

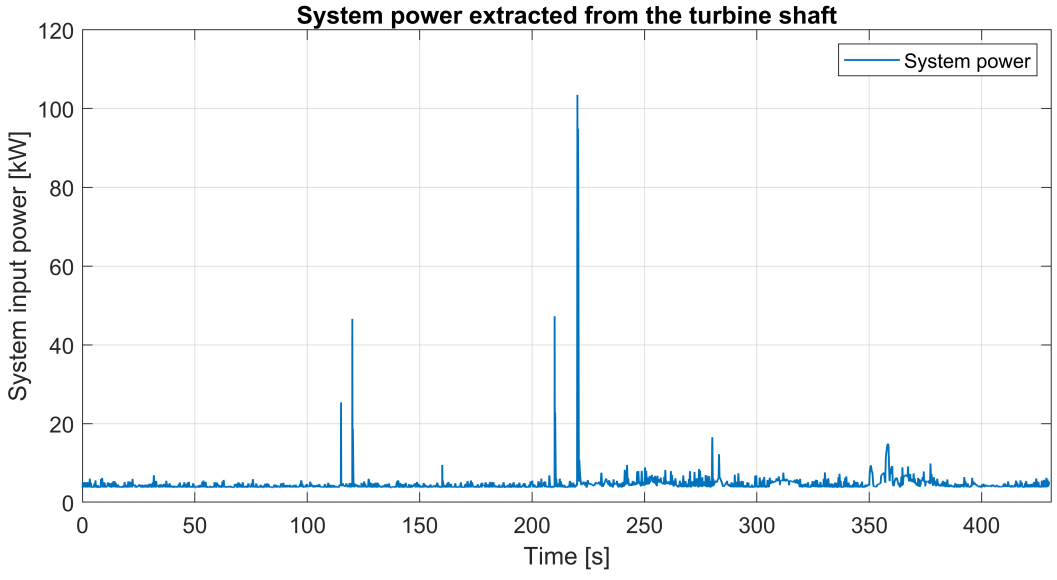


Figure 10 – Mechanical system power extracted from the turbine shaft.

### 4.4 Impact on aircraft performance

To further understand how the system attributes affect the measure of performance (fuel burn), Table 3 summarizes the fuel burned for different aircraft configurations, starting with the most basic configuration of no added vehicle systems. Flying the mission under the influence of system mass will increase the fuel burned with almost $5\ kg$. Including the influence of drag due to wing fairings (denoted "system volume" in the table) adds another $1\ kg$ of fuel burned, and lastly, taking into account the extracted energy from the turbine shaft adds an extra $0.17\ kg$ of fuel burned.

It should be clarified that the dimensions of the fairings assumes to follow the dimensions of the actuators they enclose. With the method provided by ESDU it is estimated that the fairings contribute with a mean increase in drag coefficient of $0.7$ counts of drag over the course of the flown mission. This is, for the aircraft in this study, a mean increase of merely $0.28\ \%$ in aircraft basic drag. Further, the structural mass of the aircraft remains unaltered and is assumed not to be affected by the installed equipment mass.

Table 3 – Total consumed fuel under the influence of different system aspects. The results are valid for the mission presented in Figure 8. The aircraft is assumed fully fueled at the start of the mission

| | **No systems** | **System mass** | **System mass<br>System volume** | **System mass<br>System volume<br>System energy** |
|---|---|---|---|---|
| Consumed fuel | 512.78 $kg$ | 517.61 $kg$ | 518.73 $kg$ | 518.90 $kg$ |
| **Abs. increase** | | 4.83 $kg$ | 5.95 $kg$ | 6.12 $kg$ |
| **Rel. increase** | | 0.94 % | 1.16 % | 1.19 % |

## 5. Discussion

The evaluation of an actuation system is a cumbersome task. Good knowledge on how the system is going to be used is required, both for the sake of the actuation system design and also the design of its adjacent systems. Integration of all systems into the aircraft will also matter. All this generally makes it difficult to evaluate various claimed benefits with one system solution compared to other solutions, or more specifically, electric system solutions compared with hydraulic solutions. The method raised in this paper is a first iteration to structure this task through a proposed component model structure and a breakdown of systems adjacent to the actuation system. There are plenty of methods related to evaluation of various actuation system aspects (small summary is found in [8]) and this method should therefore be seen as a complement to the other methods.

The vast amount of models covered in this paper needs further development and verification. However, as for now, they are examples that can be used as a basis on which further functionality can be built. The electrical models especially needs further refinement. The design of electrical components is highly driven by temperature aspects, which have been completely omitted in this paper. Furthermore, finding the one good correlation between the design of a component and its static attributes require either detailed physical models or a tremendous amount of data, two options which are either time consuming or generally hard to retrieve. Therefore, making use of simple scaling models can serve as a good first approximation, but at the expense of model and result fidelity. This paper made use of isometric scaling models to estimate many of the different design parameters and attributes. However, the growth of these metrics are most probably not as linear as the models suggests. Allometric growth models, or equivalent power law equations, can therefore be used instead to further increase the fidelity level of these models. However, without proper validation of the models, neither model type (isometric vs allometric) can be argued more useful.

The case study shown in the paper is, because of the above mentioned reasons, a very rough approximation of the actuation system's contrition to fuel burn. Some interesting observations can however still be made. It is indicated in the study that the total system energy consumption has a very low influence on the consumed fuel over the flown mission, despite suffering from a constant energy loss in the form of leakage. However, put in relation to what is required in terms of energy by the control surfaces, this system energy consumption is significant and the cooling system must be dimensioned almost solely for the sake of the leakage. The energy consumption's relatively low influence on the consumed fuel does indicate that energy efficiency is not a direct driver for electrification of the actuation system, at least not for the aircraft and actuation system studied in this paper. The hydraulic system energy consumption can further be seen as a worst case scenario, meaning that the most probable decrease in energy consumption entailed by an electric actuation system would have an almost negligible effect on the fuel burned. The more important properties are instead the static attributes of the system components. Given the requirements and models in this paper, these attributes for an electrified actuation system can be evaluated by relatively small means, but with limitations in fidelity level.

On the subject of energy consumption there are still advantages with an increased system energy efficiency, despite its low impact on fuel burn. An increased energy efficiency could possibly decrease the size of the installed cooling power, which could bring advantages in terms of cooling system mass and volume. This emphasizes the need to properly estimate the thermal states of all system components and the environment in which they are installed, in order to sufficiently dimension the cooling system. Likewise, proper estimation of thermal states is also important for the possible need of component heating and its respective impact on fuel burn.

Lastly, the estimated drag from the fairings showed a non-negligible influence on fuel burn, which indicates the value of estimating the total volume claimed by the systems as well. It is however hard to deduce how the remaining system volume, not enclosed in the fairings, contribute to the overall design of the aircraft and thus the total aircraft drag.

## 6. Conclusions

This article presented a first iteration of a method aimed to evaluate an actuation system's operational cost. Although the vast amount of models need further refinement, they can serve as a good basis on which further functionality can be added. Results from a case study, in which the method was used, highlights the importance of accurately estimating the mass and volume of the equipment associated with the actuation system. These attributes will have a larger impact on fuel burn in comparison to system energy consumption. Good approximation of the total system energy consumption may however still be important, but not because of its direct impact on fuel burn, but because of the required installed cooling power and the cooling system's associated mass and volume.

## 7. Contact Author Email Address

Corresponding author: Christopher Reichenwallner, christopher.reichenwallner@liu.se.

## 8. Copyright Statement



## 9. Acknowledgment

This work was funded by Vinnova, grant number 2019-02772.

## References


[1] Bossche D. The A380 Flight Control electrohydrostatic actuators, achievements and lessons learnt. *International Congress of the Aeronautical Sciences*, 2006.

[2] Maré J-C. Aerospace Actuators 1: Needs, Reliability and Hydraulic Power Solutions. 1st edition, ISTE Ltd and John Wiley Sons Inc, 2016.

[3] Wiegand C, Bullick B, Catt J, Hamstra J, Walker G and Wurth S. F-35 Air Vehicle Technology Overview. *AIAA Aviation Forum*, Atlanta, Georgia, 2018.

[4] Navarro R. Performance of an Electro-Hydrostatic Actuator on the F-18 Systems Research Aircraft. *NASA/TM-97-206224*, 1997.

[5] Jensen C, Jenney G, Dawson D. Flight Test Experience With an Electromechanical Actuator on the F-18 Systems Research Aircraft. *19th Digital Avionics Systems Conference*, Philadelphia, Pennsylvania 2000.

[6] Jianming L, Zhiyuan Y, Yuping H and Zhiguo. A Review of electromechanical actuation system for more electric aircraft. *International Conference on Aircraft Utility Systems*, Beijing, China, 2016.

[7] Zhiqiang B, Yu L and Zidong L. Flight control system architecture comprehensive evaluation based on electrical actuators for more electric aircraft. *Recent Advances in Aerospace Actuation Systems and Components*, Toulouse, France, 2018.

[8] Reichenwallner C, Larsson F, Dell'Amico A and Krus P. Evaluation Aspect Mapping for Actuation System Evaluation. *32nd Congress of the International Council of the Aeronautical Sciences*, Shanghai, China, 2021.

[9] Moog, Inc. Electromechanical Actuators datasheet. Available: `https://www.moog.com/content/dam/moog/literature/Space_Defense/Space_Access_Integrated_Systems/moog-em-heritage-actuators-datasheet.pdf`. Accessed: 2022-05-23

[10] Moog, Inc. Electromechanical Actuators datasheet. Available: `https://www.moog.com/content/dam/moog/literature/Space_Defense/Space_Access_Integrated_Systems/SAIS_Modular_EMA_Rev_0315.pdf`. Accessed: 2022-05-23

[11] Vanthuyne T. An Electrical Thrust Vector Control System for the Vega Launcher. *13th European Space Mechanisms and Tribology Symposium – ESMATS 2009*, Vienna, Austria. 2009

[12] Maré J-C. Practical Considerations in the Modelling and Simulation of Electromechanical Actuators. Actuators 2020, 9, 94. doi: 10.3390/act9040094.

[13] Kugler G. Methodology for prediction of the hydraulic systems mass and volume in during aircraft conceptual design (original title in Swedish). 2001.

[14] Gudmundsson S. General Aviation Aircraft Design: Applied Methods and Procedures. 1st edition, Elsevier Inc, 2014.

[15] Hoerner S F. Fluid-Dynamic Drag: Theoretical, Experimental and Statistical Information. 1965.

[16] ESDU 84035. Drag of stub wings and fairings on a flat plate with a turbulent boundary layer for subsonic and supersonic speeds.

[17] ESDU 77028. Geometrical Characteristics of Typical Bodies.

[18] ESDU 78019. Profile Drag of Axisymmetric Bodies at Zero Incidence for Subcritical Mach Numbers.

[19] Lars Forsell and Ulrik Nilsson. Admire the aero-data model in a research environment version 4.0, model description. FOI, 2005.